Cell-Type-Specific H^+-ATPase Activity in Root Tissues Enables K^+ Retention and Mediates Acclimation of Barley (*Hordeum vulgare*) to Salinity Stress[1][OPEN]

Lana Shabala, Jingyi Zhang, Igor Pottosin, Jayakumar Bose, Min Zhu, Anja Thoe Fuglsang, Ana Velarde-Buendia, Amandine Massart, Camilla Beate Hill, Ute Roessner, Antony Bacic, Honghong Wu, Elisa Azzarello, Camilla Pandolfi, Meixue Zhou, Charlotte Poschenrieder, Stefano Mancuso, and Sergey Shabala*

School of Land and Food, University of Tasmania, Hobart, Tasmania 7001, Australia (L.S., J.Z., I.P., J.B., Mi.Z., H.W., Me.Z., S.S.); Centro Universitario de Investigaciones Biomédicas, Universidad de Colima, Colima 28045, Mexico (I.P., A.V.-B.); Australian Research Council Centre of Excellence in Plant Energy Biology and School of Agriculture, Food, and Wine, University of Adelaide, Glen Osmond, South Australia 5064, Australia (J.B.); Department of Plant and Environmental Sciences, University of Copenhagen, Copenhagen DK-1871, Denmark (A.T.F.); Fisiología Vegetal, Facultad de Biociencias, Universidad Autónoma de Barcelona, Bellaterra 08193, Spain (A.M., C.Po.); School of BioSciences (C.B.H., U.R.) and Australian Research Council Centre of Excellence in Plant Cell Walls, School of BioSciences (A.B.), University of Melbourne, Victoria 3010, Australia; and Department of Horticulture, University of Florence, Florence 50019, Italy (E.A., C.Pa., S.M.)

ORCID IDs: 0000-0002-5360-8496 (L.S.); 0000-0003-1153-8394 (A.T.F.); 0000-0002-6754-5553 (C.B.H.); 0000-0002-6482-2615 (U.R.); 0000-0001-7483-8605 (A.B.); 0000-0001-6629-0280 (H.W.); 0000-0002-8686-8761 (C.Pa.); 0000-0003-3009-7854 (Me.Z.); 0000-0002-3818-0874 (C.Po.); 0000-0003-1752-3986 (S.M.).

While the importance of cell type specificity in plant adaptive responses is widely accepted, only a limited number of studies have addressed this issue at the functional level. We have combined electrophysiological, imaging, and biochemical techniques to reveal the physiological mechanisms conferring higher sensitivity of apical root cells to salinity in barley (*Hordeum vulgare*). We show that salinity application to the root apex arrests root growth in a highly tissue- and treatment-specific manner. Although salinity-induced transient net Na^+ uptake was about 4-fold higher in the root apex compared with the mature zone, mature root cells accumulated more cytosolic and vacuolar Na^+, suggesting that the higher sensitivity of apical cells to salt is not related to either enhanced Na^+ exclusion or sequestration inside the root. Rather, the above differential sensitivity between the two zones originates from a 10-fold difference in K^+ efflux between the mature zone and the apical region (much poorer in the root apex) of the root. Major factors contributing to this poor K^+ retention ability are (1) an intrinsically lower H^+-ATPase activity in the root apex, (2) greater salt-induced membrane depolarization, and (3) a higher reactive oxygen species production under NaCl and a larger density of reactive oxygen species-activated cation currents in the apex. Salinity treatment increased (2- to 5-fold) the content of 10 (out of 25 detected) amino acids in the root apex but not in the mature zone and changed the organic acid and sugar contents. The causal link between the observed changes in the root metabolic profile and the regulation of transporter activity is discussed.

Soil salinity is a major environmental constraint to crop production that affects about 20% of irrigated land, costing US$ 27.3 billion per year in lost revenue (Qadir et al., 2014). To date, attempts to create salt-tolerant crop germplasm have had limited success (Flowers, 2004; Shabala, 2013), largely due to the high physiological and genetic complexity of this trait. It is estimated that salinity affects transcripts of approximately 8% of all genes (Tester and Davenport, 2003), and fewer than 25% of these salt-regulated genes are salt stress specific (Ma et al., 2006). At the physiological level, numerous subtraits contribute to overall salinity tolerance, most of which are species specific and may require expression in either a particular tissue or cell type (Tester and Davenport, 2003; Shabala, 2013). It is thought that the limited success of transgenic manipulations to increase some of these traits (and, specifically, those related to ion exclusion from the shoot) is due largely to the inability to express important exclusion genes in a cell-specific manner (Roy et al., 2014).

[1]This work was supported by separate grants from the Australian Research Council and the Grain Research and Development Corporation to S.S., A.B. (grant no. CE1101007), C.B.H., and U.R.

* Address correspondence to sergey.shabala@utas.edu.au.

The author responsible for distribution of materials integral to the findings presented in this article in accordance with the policy described in the Instructions for Authors (www.plantphysiol.org) is: Sergey Shabala (sergey.shabala@utas.edu.au).

S.S. conceived the general concept and research plan; U.R., Me.Z., A.B, A.T.F., S.M., and C.Po. supervised the experiments; L.S., S.S., J.Z., J.B., I.P., Mi.Z., A.V.B., C.Pa., A.M., H.W., and E.A. conducted experiments; S.S., I.P., C.B.H., A.T.F., and U.R. critically assessed the data; S.S. wrote the article; I.P., C.B.H., U.R., A.T.F., and A.B. provided a critical assessment of the article.

[OPEN] Articles can be viewed without a subscription.

www.plantphysiol.org/cgi/doi/10.1104/pp.16.01347

While the importance of cell-specific responses for plant adaptive responses to the environment is widely accepted (Ma and Bohnert, 2007; Dinneny et al., 2008; Dinneny, 2010), only a limited number of studies have attempted to address this issue with respect to salt stress. Dinneny et al. (2008) used fluorescence-activated cell sorting to generate a genome-scale high-resolution expression map to demonstrate cell type-specific responses of various root cell types to salinity. Several thousand genes were shown to be expressed in a cell-specific manner, both in terms of longitudinal and radial root profiles (Dinneny et al., 2008). Although highlighting the complexity of plant adaptive responses to salinity, these results cannot be easily translated into breeding programs. Transcriptional changes do not necessarily reflect physiological changes (Adem et al., 2014) and thus should be interpreted with some caution. The same notion is applicable to other techniques used to reveal the tissue-specific patterning of transporter expression. For example, using a GFP fusion technique, the preferential expression of the SALT OVERLY SENSITIVE1 (SOS1) Na^+/H^+ exchanger was reported for the epidermal cells of the root tip and xylem/symplast boundary (Shi et al., 2000, 2002). Yet, the functional analysis of Arabidopsis (*Arabidopsis thaliana*) *sos1* transport mutants has revealed significant differences in root K^+ retention ability between *sos1* and wild-type plants in the mature root epidermis (Shabala et al., 2005), where no GFP signals were detected (Shi et al., 2000). At the same time, it is the function of the specific transporter/protein that ultimately determines plant adaptive responses to salinity. Therefore, there is a need to address the issue of the tissue and cell specificity of salt responses at the functional level.

Physiologically, plant adaptive responses to salinity can be grouped into four major categories: (1) dealing with the osmotic component of salt stress; (2) handling toxic Na^+ and Cl^- ions; (3) detoxifying reactive oxygen species (ROS) produced in plant tissues under saline conditions; and (4) mediating cytosolic K^+ homeostasis (Tester and Davenport, 2003; Ji et al., 2013; Shabala, 2013; Shabala and Pottosin, 2014; Flowers et al., 2015; Julkowska and Testerink, 2015; Kurusu et al., 2015). All these responses rely heavily on the regulation of transport activity across cellular membranes and, specifically, those for Na^+ and K^+ ions. High cytosolic Na^+ concentrations are considered to be toxic for cell metabolism and, thus, are reduced by various means (Tester and Davenport, 2003; Ji et al., 2013; Flowers et al., 2015). At the same time, superior K^+ retention and a cell's ability to maintain cytosolic K^+ homeostasis correlate with salinity tolerance in a broad range of plant species (Anschütz et al., 2014; Shabala and Pottosin, 2014) and are essential for preventing salinity-induced programmed cell death (Shabala, 2009; Demidchik et al., 2010). High cytosolic K^+ levels also are essential to maintain high vacuolar H^+-PPase activity, thus enabling the operation of tonoplast NHX proteins that mediate vacuolar Na^+ sequestration (Shabala, 2013). Na^+ and K^+ also are major inorganic osmolytes that confer over 70% of tissue osmotic adjustment under stress conditions (Shabala and Lew, 2002). In addition, ROS detoxification activity in plant cells is critically dependent on K^+ availability (Sun et al., 2015). This explains why the cytosolic sodium-potassium ratio is widely regarded a major determinant of plant salinity stress tolerance (Anschütz et al., 2014; Shabala and Pottosin, 2014) and why understanding the tissue specificity of its regulation may be the key to improving salinity tolerance in plants.

In this work, we address some of above gaps in our knowledge and provide a comprehensive characterization of the functional activity of the major transport systems conferring Na^+ and K^+ ionic relations in salinized plant tissues at the cell-specific level and then link it to the stress-induced changes in the tissue metabolic profile. Using barley (*Hordeum vulgare*) roots as a model system, we show that compromised K^+ retention in the root is the main detrimental factor that contributes to barley's tolerance to salinity. We show that root apical cells are much more sensitive to salt stress and attribute this differential sensitivity to superior K^+ retention in mature root epidermis originating from intrinsically higher H^+-ATPase activity (and, hence, the ability to maintain more negative membrane potential) and the reduced sensitivity of Na^+- and K^+-permeable nonselective cation channel (NSCC) to ROS generated under saline conditions.

RESULTS

Root Growth Is Arrested in a Stress-Specific Manner following the Administration of NaCl to the Root Apex But Not the Mature Root Zone

We designed a multicompartment chamber that allows for the application of different treatments to specific root zones (Fig. 1A; Supplemental Fig. S1). Compartments I to III covered the major bulk of the mature root zone, and compartment IV covered elongation and meristematic root zones (root apex; Fig. 1B). For roots grown under control conditions, all four compartments were filled with basal salts medium (BSM) solution. For stress treatment, BSM solution in either compartment II (mature zone) or IV (root apex) was replaced by either 100 mM NaCl or isotonic 170 mM mannitol solution. The roots were immobilized such that, in each zone of the root, the same surface area was exposed to the treatment (a 4-mm-long segment; Fig. 1A).

Exposure of the root apex (the first 4 mm of the root from the tip) to 100 mM NaCl resulted in an immediate arrest of root growth (Fig. 1, C and D). The same treatment applied to the mature root zone (the root segment between 14 and 18 mm from the tip) did not result in any significant ($P < 0.05$) decline in root growth compared with controls over the 3-d period of the experiment (Fig. 1, C and D). Impaired root growth was salt stress specific, as it was not observed when roots were treated with isotonic mannitol (Fig. 1, C and D). Both treatments resulted in significant accumulation of Na^+ and loss of K^+ from exposed roots ($P < 0.05$; Fig. 1E). While Na^+ accumulation was independent of the zone of salt application, roots treated with 100 mM NaCl in the apical region lost more K^+ compared with those

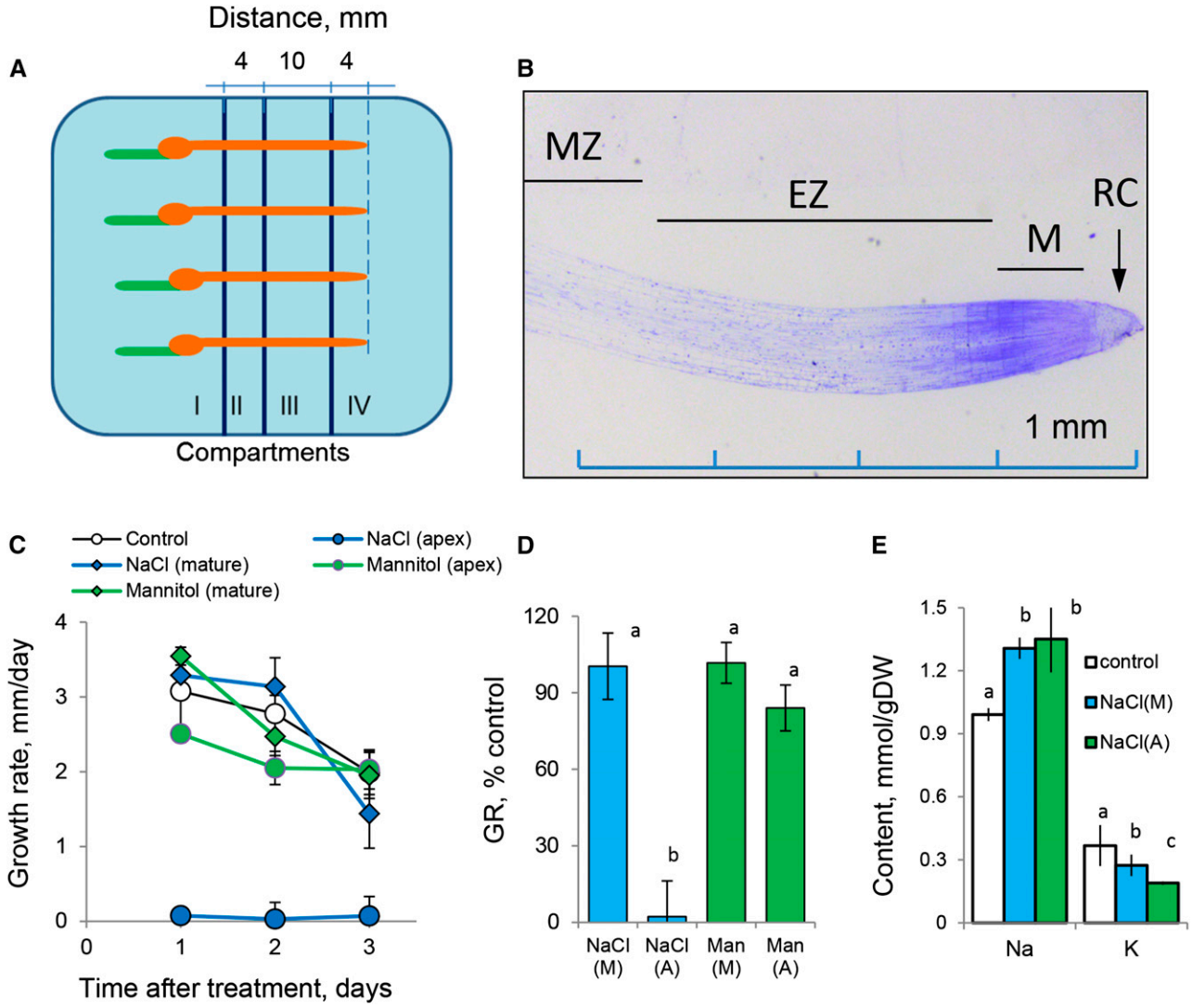

Figure 1. Barley root growth and responses to salinity (100 mM NaCl) and isotonic mannitol treatment. A, Schematic diagram depicting the experimental design and root immobilization within a multicompartment growth chamber (Supplemental Fig. S1). Salt was added to compartments II (mature zone) and IV (root apex). B, Anatomy of the barley root apex depicting functionally different root zones (modified from Shelden et al. [2016] with permission from Oxford University Press). EZ, Elongation zone; M, meristem; MZ, mature zone; RC, root cap. C, Root growth rate as a function of time after treatment. Values shown are means ± SE (n = 8–12). D, Relative growth rate (GR; % of control). E, Total root Na^+ and K^+ content after 3 d of 100 mM NaCl application to either apical or mature root zones. Values shown are means ± SE (n = 5–8). (A), Apex; DW, dry weight; (M), mature zone; Man, mannitol. Different lowercase letters indicate significant differences between treatments at $P < 0.05$.

treated in the mature zone ($P < 0.05$; Fig. 1E). This difference could not be attributed to the potential dilution effect in growing roots, as higher K^+ content was measured in the bulk of the roots still undergoing growth (where salt treatment was applied to a part of the mature zone; blue bars in Fig. 1E) but not in the roots with arrested growth (apical treatment; green bars in Fig. 1E). Thus, the dilution effect (if any) may lead only to the potential underestimation of the difference in K^+ uptake or retention ability between two zones.

The reported differences in ion accumulation are not related to the differences in root lignification between these two regions (data not shown), and such K^+ loss was not observed in mannitol-treated roots (data not shown). Taken together, the results suggest that (1) root apical tissues are much more sensitive to salinity and are immediately growth arrested upon salinity treatment and (2) the above effect is salt stress specific and may be related to a differential ability of root tissues to retain K^+ rather than restrict Na^+ uptake.

Differential Sensitivity in Growth Responses Is Not Related to Higher Na^+ Accumulation in the Root Apex

Upon acute NaCl stress, salinity-induced net Na^+ uptake was about 4-fold higher in the root apex compared

with the mature zone (Fig. 2A). However, this difference was transient, lasting less than 10 min, with fluxes gradually reduced to near-zero levels. Confocal imaging using CoroNa Green fluorescent dye revealed that, despite net Na^+ uptake being higher in the root apex upon stress onset, mature root cells accumulated more Na^+ (Fig. 2, B–H) compared with apical cells when exposed to prolonged (3-d) salinity treatments. The intensity of the fluorescence signal was much brighter in mature (Fig. 2B) compared with apical (Fig. 2D) root zones. In quantitative terms, a 2-fold higher fluorescent signal was measured from both vacuolar and cytosolic compartments in the mature root zone compared with apical cells (Fig. 2F; significant at

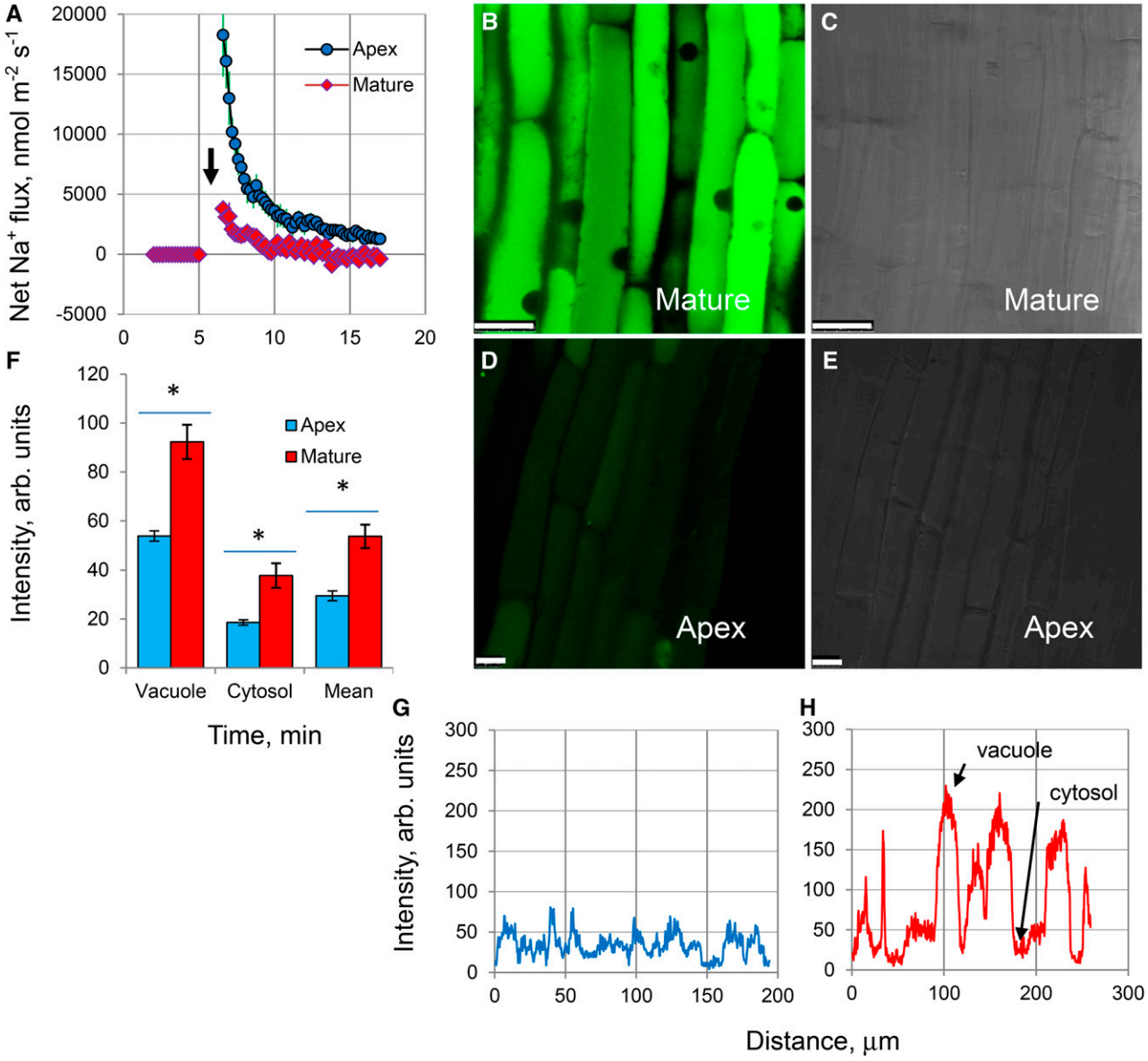

Figure 2. Na^+ uptake and accumulation in barley roots. A, Kinetics of net Na^+ fluxes measured from the epidermal root cells in the apical and mature regions in response to 100 mM NaCl treatment (indicated by the arrow). Values shown are means ± SE (n = 6–8). B and D, Na^+ accumulation and intracellular distribution in mature (B) and apical (D) root zones visualized by the CoroNa Green fluorescent dye after 3 d of 100 mM NaCl treatment. One typical image (of eight) for each zone is shown. All images were taken using the same settings and exposure times to enable direct comparisons. C and E, Bright-field images of the corresponding zones for B and D, respectively. Bars in B to D = 25 μm. F, Mean CoroNa Green fluorescence intensity measured from cytosolic and vacuolar compartments. Values shown are means ± SE (n = 70–300). Asterisks indicate significant differences between zones at $P < 0.05$. G and H, Typical examples of the spatial cross-sectional profiles of CoroNa Green fluorescence signals from roots in apical and mature root zones, respectively. Several lines were drawn across the so-called region of interest in an appropriate root zone, and continuous fluorescence intensity distribution profiles were obtained by LAS software and plotted.

$P < 0.05$). Thus, the arrest of root growth upon exposure of the apical tissue to salt (Fig. 1) cannot be explained by an accumulation of Na^+ in the root apex. Also, the ratio of fluorescent dye intensity between the vacuolar and cytosolic compartments was very similar for both apical and mature tissue (2.89 ± 0.24 versus 2.45 ± 0.19; not significant at $P < 0.05$), suggesting no difference in vacuolar Na^+ sequestration ability.

Apical Cells Have Lower H^+-Pumping Ability, Are More Depolarized, and Retain Less K^+ When Exposed to Salinity

Salinity treatment resulted in a significant membrane depolarization of epidermal cells (by 74 ± 2 mV; Fig. 3A). The intrinsic (steady-state) membrane potential (MP) values of mature cells in controls were much more negative compared with apex cells (−128 ± 3.9 mV versus −111 ± 3.1 mV, respectively; $P < 0.01$; Fig. 3A). Also, cells in the mature zone showed higher potency for repolarization. As a result, the new steady-state MP values under saline conditions were nearly 40 mV more negative in the mature zone (−96 ± 2.3 mV versus −58 ± 1.8 mV, respectively; $P < 0.01$; Fig. 3A). Physiologically, this difference in steady-state values is critical to determining plant ionic balance and was expected to be reflected in the cell's ability to retain K^+ by controlling either depolarization-activated outward-rectifying (GORK in Arabidopsis) K^+ channels (Véry et al., 2014) or any nonselective cation channel, active at depolarized potentials (Demidchik and Maathuis, 2007). Indeed, while a substantive peak K^+ efflux of approximately 2,100 nmol m^{-2} s^{-1} was measured from the root apex in response to 100 mM NaCl treatment (Fig. 3B), this efflux was only approximately 80 nmol m^{-2} s^{-1} in cells in the mature zone. Furthermore, the steady-state fluxes before and after salinity treatment were significantly ($P < 0.01$) different, with a 7.5-fold difference in net K^+ flux reported between the two zones 20 min after NaCl application (−600 ± 116 versus −80 ± 32 nmol m^{-2} s^{-1}, respectively; Fig. 3B; significant at $P < 0.01$). This may explain the difference in the overall root K^+ content between treatments reported in growth experiments (Fig. 1E).

The PM H^+-ATPase is known to be a major determinant of MP (Palmgren and Nissen, 2011); thus, more negative MP values in mature root zones could be a direct consequence of a more active H^+ pump. To test this, PM vesicles were purified from the root apex and mature zone of control- and salt-grown plants, followed by an H^+-ATPase activity assay using a fluorescent 9-amino-6-chloro-2-methoxyacridine (ACMA) probe. ACMA accumulates in an impermeable form inside vesicles upon protonation, with a decrease in fluorescence directly correlated to the amount of H^+ transported into the vesicles. Cells in the mature zone exhibited a higher H^+-pumping capacity compared with apex cells, as indicated by the slope of the curve after H^+-ATPase activation by Mg^{2+} (Fig. 3C). Salinity treatment decreased the H^+-ATPase activity in both zones; however, the H^+-ATPase activity was much higher in the mature zone (Fig. 3C). Taken together, we conclude

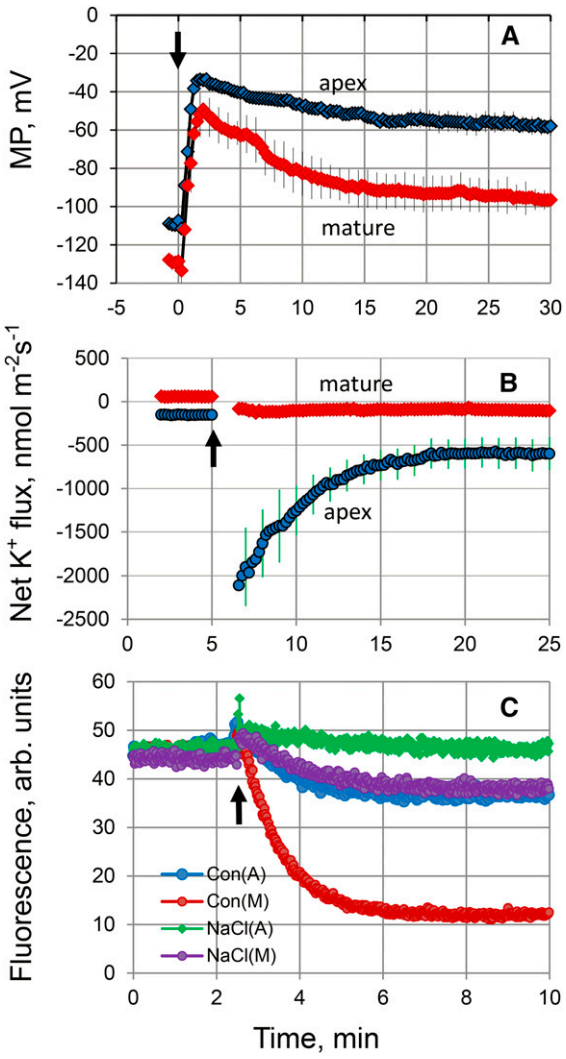

Figure 3. Superior K^+ retention in the mature root zone is attributed to an intrinsically higher rate of H^+-ATPase extrusion activity. A, Changes in the plasma membrane (PM) potential in epidermal root cells in two different zones upon exposure to 100 mM NaCl (indicated by the arrow). Values shown are means ± SE (n = 6–8). B, Net K^+ fluxes measured from the epidermal root cells in the apical and mature zones in response to 100 mM NaCl treatment (indicated by the arrow). Values shown are means ± SE (n = 7–10). C, H^+ pumping measured by ACMA quenching. PMs containing the H^+-ATPase were incubated with ATP, and H^+ pumping was activated by the addition of Mg^{2+} (indicated by the arrow). This experiment is representative of three independent PM purifications.

that the higher sensitivity of the root apex to salinity is related to its poor K^+ retention ability, which originates from a lower H^+-ATPase activity and, hence, inability to maintain a sufficiently negative MP.

Higher Sensitivity of the Root Apex to Salinity May Be Related to a Higher ROS Accumulation and a Larger Density of ROS-Activated Cation Current

Salinity stress results in a rapid production of ROS (Mittler, 2002). Indeed, root treatment with 100 mM NaCl

resulted in significant accumulation of ROS in barley roots (Fig. 4). However, this salt-induced accumulation was highly tissue specific and observed only in the root apex (Fig. 4, A, B, and E) and, specifically, in the elongation zone (Fig. 1B). In contrast, a decrease of fluorescence was observed in the mature root zone under salt stress (Fig. 4, C–E). While the salt-induced increase in ROS accumulation in the apical zone was NaCl specific and was not observed in roots exposed to isotonic sorbitol treatment (Fig. 4F), the quenching of the fluorescence in the mature root zones was nonspecific (i.e. activated by both NaCl and sorbitol; Fig. 4, E and F).

This accumulation of ROS in the elongation zone of salinized roots may have major implications for intracellular ionic homeostasis. By interacting with transition metals such as either copper or iron, increased accumulation of hydrogen peroxide (H_2O_2) may result in the formation of highly reactive hydroxyl radicals ($OH^\bullet$) in both the apoplast (Demidchik, 2015) and cytosol (Rodrigo-Moreno et al., 2013). Both H_2O_2 and $OH^\bullet$ may cause a major perturbation in intracellular ionic homeostasis by activating a range of cation-permeable ion channels (Demidchik and Maathuis, 2007; Demidchik et al., 2010; Shabala and Pottosin, 2014). Thus, tissue-specific salinity stress sensitivity between the root apex and mature zones may be causally related to the patterns of $OH^\bullet$ production and/or sensitivity of membrane transporters to $OH^\bullet$. Consistent with this hypothesis, the application of an $OH^\bullet$-generating copper/ascorbate mix resulted in a rapid and substantive Ca^{2+} uptake and K^+ efflux from barley roots (Fig. 5). Both responses were 1 order of magnitude higher in the root apex compared with the mature root zone. This suggests that increased production of ROS, which is able to induce greater K^+ loss from the root apex as compared with the mature zone, may be the cause of the higher salt sensitivity of the former tissue.

To elucidate the nature of membrane transporters mediating these pronounced K^+ and Ca^{2+} fluxes, we conducted a series of patch-clamp experiments, targeting

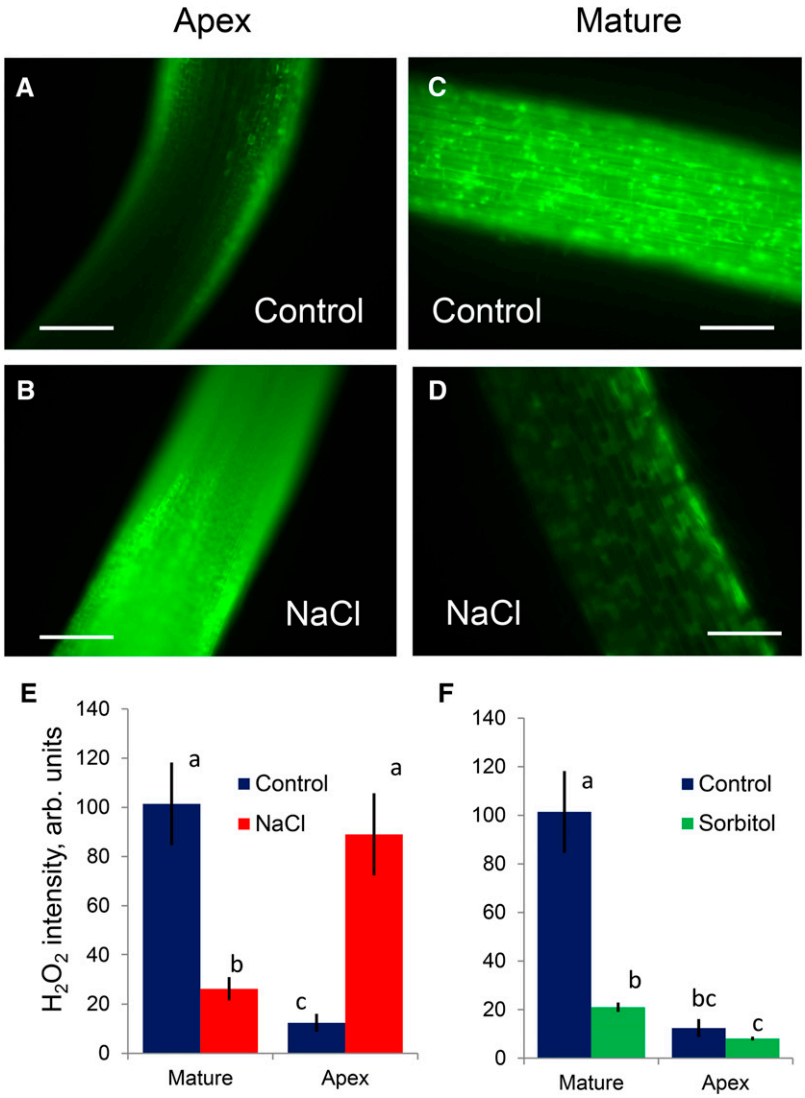

Figure 4. Stress-induced ROS accumulation in barley roots visualized by 2′,7′-dichlorofluorescein diacetate staining (for details, see Rodrigo-Moreno et al., 2013). A to D, Representative images (out of eight) of mature (approximately 20 mm from the tip) and apical (2 mm) zones from control and salt-treated (100 mM NaCl for 24 h) roots. Bars = 200 μm. E, Average fluorescence signal intensity from the apical and mature root zones (in arbitrary units) for control and stressed roots. Values shown are means ± SE ($n = 8$). F, As for E, but for roots treated with isotonic mannitol solution. Data labeled with different lowercase letters are significantly different at $P < 0.05$.

$OH^{\bullet}$-induced currents, known to confer K^+ and Ca^{2+} transport across the root PM. Consistent with previous observations, the $OH^{\bullet}$-induced current was biphasic, composed of the instantaneous and the time-dependent depolarization-activated components (Fig. 6A), which could be tentatively assigned to ROS-activated NSCC and GORK, respectively (Demidchik et al., 2014; Shabala and Pottosin, 2014). Due to a strong outward rectification, a reversal potential of the time-dependent current could not be defined unequivocally; instantaneous currents reversed around −30 mV (i.e. between equilibrium potentials for K^+ and Cl^-), supporting previous observations of its nonselective nature in accordance with Velarde-Buendía et al. (2012). Both instantaneous and time-dependent $OH^{\bullet}$-induced currents were significantly higher in the apical zone. Total (instantaneous plus time-dependent) outward K^+ current was approximately 3-fold higher in the root apex compared with the mature zone (Fig. 6B). Surprisingly, the addition of 80 mM NaCl had either no or little effect on the magnitude of $OH^{\bullet}$-induced currents and the reversal potential of the instantaneous current (Fig. 6A). This implies (1) a low discrimination between Na^+ and Cl^- of the instantaneous current and (2) that its conductance was already saturated at lower saline. Thus, any difference in the NSCC amplitude, observed between the apex and mature root zones, more likely should be attributed to a difference in the surface expression of ROS-activated ion transporters rather than their differential sensitivity to ROS.

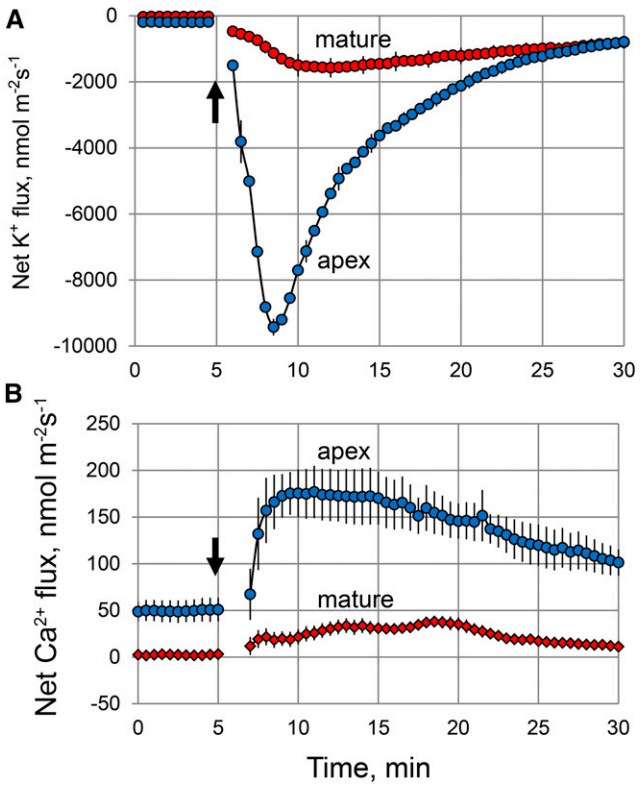

Figure 5. Net K^+ (A) and Ca^{2+} (B) fluxes measured from epidermal root cells in response to an $OH^{\bullet}$-generating copper/ascorbate (0.3/1 mM) mixture applied at 5 min (indicated by the arrows). Values shown are means ± SE (n = 6–8).

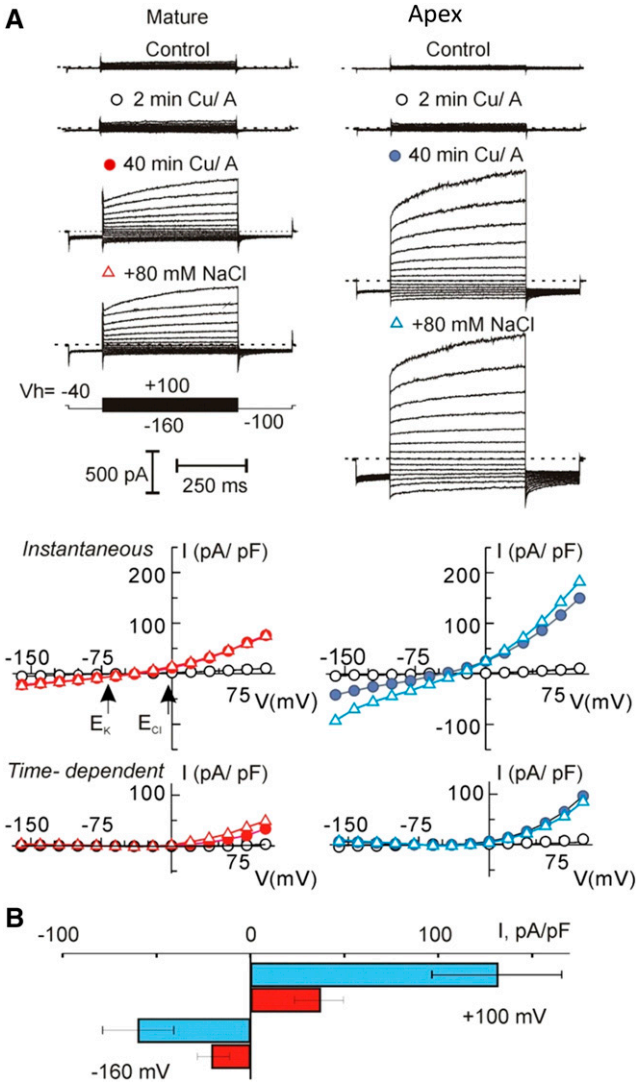

Figure 6. ROS induced nonselective current in protoplasts from elongation and mature root zones. A, Examples of whole-cell recordings of membrane currents, induced by $OH^{\bullet}$ in two protoplasts of equal size (capacitance = 5.5 pF), isolated from mature or elongation root zones. Ionic concentrations are given in "Materials and Methods." Respective current (I)/voltage (V) curves for instantaneous and time-dependent current components at the beginning of treatment (2 min), 40 min after, and after a subsequent addition of 80 mM NaCl are presented. Arrows indicate equilibrium potentials for K^+ and Cl^- for standard bath and pipette solutions. Cu/A, Copper/ascorbate. B, Mean density of total (instantaneous plus time-dependent) inward and outward ROS-induced currents, measured at −160 mV and +100 mV, respectively, after 40 min of treatment in a standard bath solution. Values shown are means ± SE; n = 18 and 15 for elongation and mature zones, respectively.

Root Metabolites Are Altered in the Root Apex after Salinity Stress

Using gas chromatography-mass spectrometry (GC-MS), 75 metabolites in both apical and mature root

zones were semiquantified before and after salinity stress; only statistically significant (Student's t test, $P < 0.05$) metabolite changes will be discussed (Table I). Root treatment with 100 mM NaCl for 24 h increased (2- to 5-fold) the content of 10 (out of 25 detected) amino acids in the root apex (Table I). By contrast, no changes were reported in the root amino acid profile in the mature zone. The root apex also displayed a significant increase of seven (out of 16) organic acids, with particularly high fold changes detected for citrate and malate (16- and 27-fold, respectively) and allantoin (6.7-fold). None of these changes were detected in the mature root zone. The metabolite profile of the apical tissue also showed a strong decrease in the levels of sugars and sugar derivatives (five of 13 analyzed compounds); but with the exception of Fru, none of these changes were significant in the mature zone (Table I). Overall, out of 75 metabolites analyzed, significant changes were detected for 30 in the apical tissue but only for four in the mature root zone.

Table I. *Tissue-specific changes in the metabolite profile of barley roots in response to 100 mM NaCl treatment*

Only metabolites showing significant (at $P < 0.05$) changes in one of the zones are shown. Numbers shown in boldface indicate significant ($P < 0.05$) differences compared with the controls.

Metabolite	Fold Change	
	Mature	Apex
Increased (apex)		
Amino acids		
Asp	1.46	**2.75**
Asn	−1.61	**4.3**
Glu	1.17	**5.16**
Gly	1.6	**5.99**
His	−2.70	**2.76**
Lys	1.25	**5.15**
Orn	3.05	**5.83**
Ser	1.90	**2.17**
Thr	1.35	**4.05**
Organic acids		
Citrate	2.44	**16.78**
Ferulate	1.09	**6.36**
Fumarate	1.45	**2.70**
Quinate	−1.85	**1.95**
Threonate	−1.89	**1.97**
Malate	−1.11	**27.48**
Sugars and derivatives		
Suc	−1.09	**1.92**
Glycerate	−1.37	**1.40**
Other compounds		
Allantoin	1.33	**6.65**
Ethanolamine	1.38	**3.27**
Decreased (apex)		
Amino acids		
Leu	**−2.04**	**−2.08**
Trp	**−5.88**	**−2.22**
Organic and fatty acids		
Erythronate	−1.85	**−1.61**
Sugars and derivatives		
Fru	**−12.5**	−4.0
Galactinol	−12.5	**−3.57**
Inositol	1.52	**−2.27**
Threitol	−1.75	**−3.03**
Glc-6-P	1.67	**−4.55**
Glc	−1.79	**−6.67**
Mixed responses		
Amino acids		
Phe	**2.54**	**−2.94**

Exogenous Application of Allantoin Reduced the Extent of ROS-Induced K^+ Loss from Barley Roots

As shown in Table I, one of the most pronounced metabolic alterations observed in stressed roots was a very significant (6-fold) increase in the level of allantoin in the root apex. Given the recent reports for the mitigating role of allantoin in oxidative stress damage in plants (Watanabe et al., 2014), we tested the effects of exogenously supplied allantoin on root ion flux responses to ROS. Root pretreatment with a physiologically relevant (1 mM) concentration of allantoin reduced the sensitivity of the root apex to both salinity and ROS stresses (Fig. 7). The peak net K^+ efflux was reduced about 2-fold in allantoin-treated roots exposed to H_2O_2 stress (Fig. 7); this reduction was 3-fold in the case of roots treated with 100 mM NaCl (Fig. 7B).

DISCUSSION

To assist in the interpretation of a complex data set that highlights the importance of tissue-specific responses to salt treatment, we have provided a model to explain the differential sensitivities between the apical and mature root tissues at the molecular level (Fig. 8).

Compromised K^+ Retention But Not Differences in Na^+ Accumulation or Exclusion Ability Confers Higher Salt Sensitivity to the Root Apex

The retention of stable K^+ concentrations in the cytosol is required to balance the toxic effects of Na^+ accumulation (Anschütz et al., 2014; Shabala and Pottosin, 2014). We demonstrate that the higher salt sensitivity of the root apex was not related to higher Na^+ accumulation in root tissues but rather originated from the compromised capacity for K^+ retention in the root apex.

A lower Na^+ accumulation in the root apex may be expected in the light of the predominant expression of SOS1 Na^+/H^+ exchangers in the root apex (Shi et al., 2000); hence, the roots' Na^+ exclusion ability should be higher in this zone. Indeed, CoroNa Green fluorescence data suggest that, under long-term salinity exposures, root apical cells (and, specifically, cells in the elongation zone) accumulate less sodium compared with those in the mature region of the root (Fig. 2). Yet, despite this more pronounced Na^+ exclusion ability, root apical cells were much more sensitive to salinity, and root growth of the apex was completely arrested upon NaCl treatment (Fig. 1).

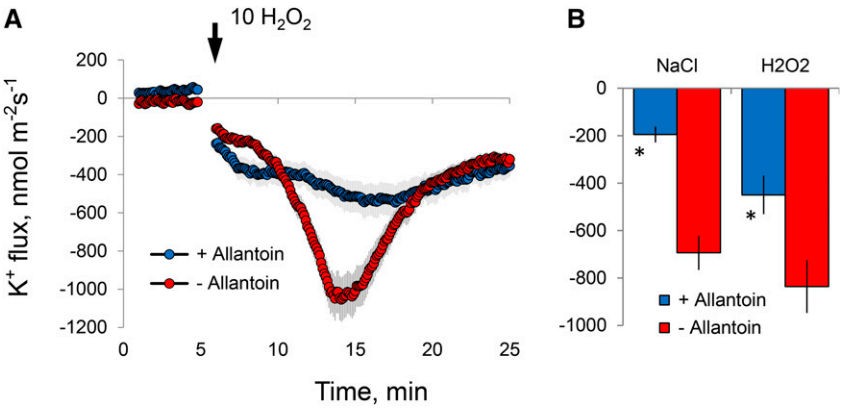

Figure 7. Effects of root pretreatment with 1 mM allantoin (for 24 h) on K^+ flux responses measured from epidermal root cells in the elongation zone upon exposure to salinity and oxidative stresses. A, Transient net K^+ flux kinetics in response to 10 mM H_2O_2. B, Peak K^+ flux values caused by acute salinity (100 mM NaCl) and oxidative (10 mM H_2O_2) stresses. Values shown are means ± SE (n = 5–6). Asterisks indicate significant differences compared with the nonpretreated control at $P < 0.05$.

Contrary to long-term trends, immediately upon salinity exposure, net Na^+ influx was much higher in the apex (Fig. 2A). This could explain the approximately 40-mV difference in membrane depolarization between apical and mature root zones upon NaCl treatment (Fig. 3A), with major consequences to K^+ retention and cytosolic K^+ homeostasis (Fig. 3B), as NaCl-induced K^+ efflux in plant roots is mediated mainly by GORK channels that display very strong voltage dependence and are activated by membrane depolarization (Fig. 8; Anschütz et al., 2014).

Cell elongation depends on the cell's ability to maintain turgor pressure and, thus, the uptake of osmolytes and water by vacuoles. Sodium and potassium are two major inorganic osmolytes contributing up to 65% of cell turgor recovery in osmotically stressed Arabidopsis roots (Shabala and Lew, 2002). In this study, the total sum of Na^+ and K^+ was not significantly different between the mature root zone and the apex (Fig. 1E). Thus, the difference in turgor may not be the cause of the arrested root growth (Fig. 1, C and D) upon the apical treatment. Therefore, the difference in the K^+ retention between the two zones needs to affect the growth in a more specific manner. This is further supported by the stress specificity of the observed effects, which were not present when isotonic mannitol concentrations were used (Fig. 1E). Mannitol treatment did not result in membrane depolarization but instead led to a slight hyperpolarization of the PM (Shabala and Lew, 2002) and resulted in an increased net K^+ uptake in both Arabidopsis (Shabala and Lew, 2002) and barley (Chen et al., 2005) roots. Consequently, upon mannitol treatment, no significant growth difference was observed between the apex and the mature zone (Fig. 1, C and D). The process of cell elongation is not just a mechanical expansion but, instead, is an orchestrated process involving cell wall weakening and the synthesis of organelles and other cellular components. One may assume that the higher net K^+ efflux (Fig. 3B) implies a lower cytosolic K^+ (for direct evidence in Arabidopsis, see Shabala et al., 2006), which could alter some of these processes, hence affecting the overall growth rate. In the longer term, an imbalance between root and shoot growth would affect the roots' ability to supply water and nutrients to match shoot demands, with the consequent growth and yield penalties.

Intrinsically Higher H^+-ATPase Activity Is Essential to Confer Higher Salinity Tissue Tolerance in the Mature Root Zone

High cytosolic K^+ levels required to provide optimal conditions for cell metabolism are achieved primarily by the maintenance of a large (−120 to −180 mV) negative voltage difference across the PM (Shabala and Pottosin, 2014). This resting potential is set by the PM H^+-ATPase and is normally kept close to the equilibrium potential for K^+ (Hirsch et al., 1998). Under salinity, the membrane depolarizes following the influx of positively charged Na^+ ions, which shifts membrane potential values above the equilibrium potential for K^+ and results in significant outward K^+ currents (Anschütz et al., 2014; Véry et al., 2014). This shift also implies that K^+ uptake may occur via active transport only. Intrinsically higher H^+-ATPase activity is essential to prevent this shift and to fuel the active K^+ uptake via H^+-coupled cotransport. Strong positive correlation between H^+-ATPase activity and salinity stress tolerance has been reported for several species (Bose et al., 2015), including barley (Chen et al., 2007). Here, we show that this can also explain the differential K^+ retention (and overall salinity stress sensitivity) between apical and mature root tissues (Fig. 3).

Could ROS Contribute to a Poorer K^+ Retention?

Salt-induced Na^+/K^+ exchange across the plasma membrane is mediated by GORK and NSCC (Fig. 8; Shabala and Pottosin, 2014). A large contribution of NSCC is confirmed by the fact that Gd^{3+}, a known blocker of NSCC, caused a 60% inhibition of NaCl-induced K^+ efflux (Supplemental Fig. S2). ROS (reflecting mainly, but not specifically, H_2O_2 levels) production under salt stress was substantially higher in the elongation zone (Fig. 4). H_2O_2 from either side of the membrane will activate inward-rectifying NSCC, mediating Ca^{2+} influx in the root elongation zone (Demidchik et al.,

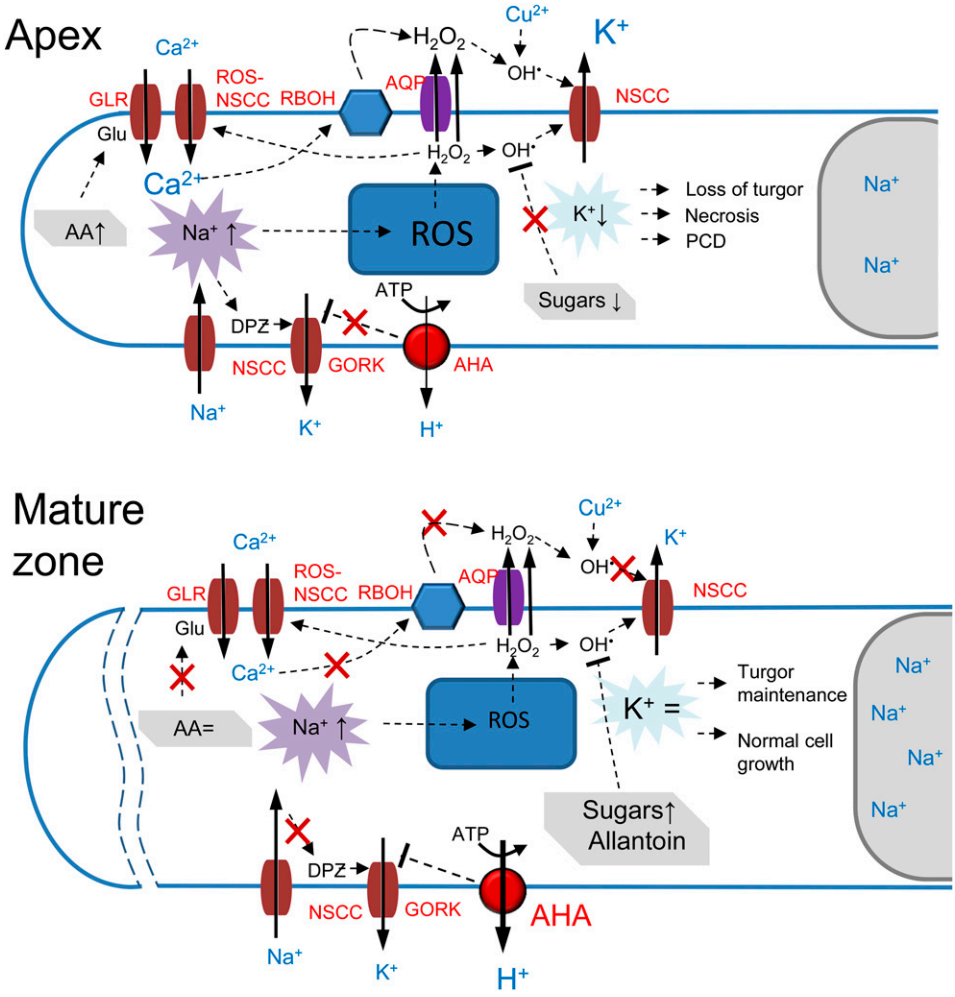

Figure 8. A model to explain the differential sensitivity to salt stress between apical and mature root tissues. Abbreviations in red define specific PM transporters involved: APA, P_2B-type H^+-ATPase; AQP, aquaporin; RBOH, NADPH oxidase. A, In the root apex, Na^+ transport across the PM is mediated by NSCC and results in a significant membrane depolarization (DPZ), leading to GORK activation and a massive efflux of K^+ from the cytosol. Increased Na^+ uptake also results in an increased ROS (H_2O_2) production in mitochondria. H_2O_2 then moves to the cytosol and is transported to the apoplast (cell wall) either by diffusion or via aquaporin, where it interacts with the transition metal (Cu^{2+} in the model), resulting in the formation of $OH^{\bullet}$. The latter activates NSCC from the apoplastic side, resulting in further K^+ loss from the cell. The cytosolic mode of NSCC activation by $OH^{\bullet}$ also is possible. Elevation in cytosolic Na^+ also results in an elevated cytosol-free Ca^{2+} pool and stimulates NADPH oxidase activity, resulting in a further increase in H_2O_2 accumulation in the apoplast. Stress-induced increases in the amino acid (AA) pool (and, specifically, in Glu) stimulates additional Ca^{2+} uptake via GLR, leading to more H_2O_2 production by NADPH oxidase. The massive K^+ loss mediated by these three concurrent mechanisms results in the loss of cell turgor (and, hence, root growth arrest) and, depending on the severity of salt stress, either programmed cell death (PCD) or necrosis in the root apex. B, In the mature root zone, intrinsically higher H^+-ATPase activity reduces the extent of depolarization and prevents the activation of GORK. The observed increase in the sugar levels ensures efficient nonenzymatic scavenging of $OH^{\bullet}$, thus preventing K^+ efflux via $OH^{\bullet}$-activated NSCC. The ROS-induced activation of K^+ efflux pathways also is prevented by allantoin. The constant level of the amino acid pool ensures the absence of the activation of GLR and results in a lesser formation of H_2O_2 by NADPH oxidase. Together with the higher vacuolar Na^+ content, these cells maintain normal turgor and metabolism and do not undergo programmed cell death.

2007). On the other hand, the highly reactive $OH^{\bullet}$, formed upon H_2O_2 reduction by Fe^{2+} or Cu^+, causes membrane depolarization and the activation of GORK and a variety of nonselective conductances, culminating in a massive K^+ efflux (Demidchik et al., 2010; Shabala and Pottosin, 2014). The $OH^{\bullet}$-induced K^+ current was 3-fold higher in the protoplasts from the elongation zone (Fig. 6). Combined with a larger depolarization (Fig. 3A) and, hence, higher driving force for K^+ efflux, this would contribute to an even higher potentiation of net K^+ efflux in this zone (Fig. 5A). The $OH^{\bullet}$-induced K^+ efflux in the root mature zone of barley varieties with contrasting salt sensitivities was not significantly different. Yet, in the background of elevated external polyamines, $OH^{\bullet}$-induced

K^+ efflux was greatly potentiated in salt-sensitive and, to a much lesser extent, salt-tolerant varieties (Velarde-Buendía et al., 2012). Upon salt stress, polyamines could be exported to the apoplast and oxidized there, forming H_2O_2 by cell wall-associated amine oxidase (Rodríguez et al., 2009). However, H_2O_2 also can cross the membrane by free diffusion or via aquaporins (Verdoucq et al., 2014). Once occurring in the apoplast, it could be reduced by either copper-containing (diamine oxidase) or iron-containing (polyamine oxidase) centers to $OH^\bullet$ (Fig. 8; Liszkay et al., 2004; Pottosin et al., 2014). On the other hand, copper import by specific transporters increases cytosolic $OH^\bullet$ generation and the activation of NSCC, mediating K^+ release in vivo (Rodrigo-Moreno et al., 2013). Therefore, the effects of ROS in membrane conductance are not only defined by the tissue-specific expression of ROS-sensitive transporters but are contextual and depend on ROS interconversion and transport as well as interaction with other factors (e.g. polyamines; Fig. 8). In the case of $OH^\bullet$, which activates a plethora of K^+-release channels, the comparative efficiency of either internal or external action sites also would be dependent on the $OH^\bullet$-scavenging activity, which is much higher in the cytosol than in the apoplast.

$OH^\bullet$ cannot be scavenged by enzymatic antioxidants and can be reduced only by nonenzymatic means, with sugars and sugar alcohols playing a pivotal role in nonenzymatic ROS scavenging (Keunen et al., 2013). Here (Table I), we show that the sugar and sugar alcohol levels decreased dramatically in the apex, but only Fru and galactinol were decreased in the mature zone tissues. This may suggest that the reported difference in ROS sensitivity between the two different tissue types may be partially explained by the difference in nonenzymatic $OH^\bullet$-scavenging potential.

Furthermore, various plants respond to environmental stresses by activating enzymes, resulting in increased levels of allantoin and allantoate (Sagi et al., 1998). Recently, the constitutive accumulation of allantoin was shown to improve overall plant performance under stress by activating abscisic acid signaling pathways (Wang et al., 2012), and exogenous application mitigated oxidative damage symptoms (Watanabe et al., 2014). Here, we show that pretreating barley roots with physiologically relevant concentrations of exogenously applied allantoin desensitized the root apical tissues and increased their ability to retain K^+ upon both salinity and ROS exposure (Fig. 7). In this context, the increased levels of allantoin in the ROS-sensitive root apical cells may be interpreted as the plant's attempt to prevent stress-induced K^+ loss. This increase in allantoin is not required in the mature zone, where stress-induced ROS production is not observed (Fig. 4).

Changes in Primary Metabolism Exacerbate Differential K^+ Retention between Tissues

Salt treatment caused a clear change of the levels of sugars, tricarboxylic acid cycle metabolites, and amino acids in the root apex but not in mature tissue (Table I). Elevated amino acid levels are commonly associated with increased tissue damage caused by salinity (Widodo et al., 2009) and protein degradation (Dubey and Rani, 1990) and are believed to be a nonspecific reaction to salt stress rather than a plant response associated with tolerance (Hill et al., 2013). The largest amino acid increase was for Orn (5.83-fold in the apex; Table I). Physiologically relevant concentrations of Orn have been shown to result in an increased stress-induced K^+ efflux from roots (Cuin and Shabala, 2007), which could explain the poor K^+ retention ability in the root apex reported in this study.

We also detected a strong increase in Glu (5.16-fold) and Gly (5.99-fold) levels in the root apex. Plant glutamate receptor-like (GLR) genes are closely related to mammalian ionotropic Glu receptors (Price et al., 2012), which operate as Glu- and Gly-gated NSCCs that catalyze the uptake of K^+, Na^+, and Ca^{2+} into neurons (Sohn, 2013). Plant GLRs were confirmed recently to be NSCC (Price et al., 2012; Forde, 2014). Therefore, activated by Glu, GLR may mediate stress-induced Ca^{2+} uptake, with a consequent rise in cytosolic Ca^{2+}, that in turn can activate the plasma membrane NADPH oxidase (Lecourieux et al., 2002), leading to elevated H_2O_2 levels and a consequent formation of $OH^\bullet$ (as discussed above), leading to a massive K^+ efflux via $OH^\bullet$-activated outward-rectified (GORK) K^+ channels (Demidchik et al., 2010). Thus, the strong increase in Glu levels found in the root apex (Table I) may be an additional factor exacerbating a stress-induced decrease in the cytosolic K^+ pool in this zone, leading to the activation of caspase-like enzymes and, finally, programmed cell death (Fig. 7). Ser, found to have increased (2.17-fold) in the root apex, also is known to be capable of activating GLRs in plants (Stephens et al., 2008).

MATERIALS AND METHODS

Plant Material and Growth Conditions

Barley seeds (*Hordeum vulgare* 'CM72') were obtained from the Australian Winter Cereals Collection. Seeds were surface sterilized with 1% HClO for 15 min and rinsed thoroughly with distilled water. Plants were grown hydroponically in aerated BSM solution containing 0.5 mM KCl, 0.1 mM $CaCl_2$, and 1 mM NaCl (pH 5.9) in the dark at room temperature (24°C ± 1°C). Four-day-old seedlings, with 70- to 80-mm long roots, were used for laboratory experiments.

Growth Experiments

Barley roots were immobilized in a multicompartment 120-mL chamber made of a rectangular 120- × 120-mm petri dish with built-in Perspex partitions (Supplemental Fig. S1). Narrow grooves were cut into the partitions to align roots. Grooves were sealed with petroleum jelly to prevent any solution mixing between compartments (validated using dyes; Supplemental Fig. S1). Appropriate solutions were added to each of the four compartments (I–IV; Fig. 1A), and root length was measured daily for the entire duration of the experiment (3–4 d). Three seminal roots from the same plant were placed in each groove, and their tips were aligned to protrude precisely at the same distance (5 mm) into compartment IV.

Tissue Ion Content Analysis

Root samples were rinsed quickly with 10 mM $CaCl_2$ to remove apoplastic Na^+, blotted dry with paper towels, and dried at 65°C in a Unitherm Dryer to

constant weight. Samples were then ground and digested in 10 mL of 98% H_2SO_4 and 3 mL of 30% H_2O_2 for 5 h. The digested samples were diluted with distilled water to the required volume, and root Na^+ and K^+ contents were analyzed using a flame photometer (Corning 410C).

Noninvasive Ion Flux Measurements

Net K^+, Ca^{2+}, and Na^+ fluxes were measured from apical (approximately 3 mm from the tip) and mature (approximately 20 mm) root zones using noninvasive microelectrode ion flux estimation (University of Tasmania). Briefly, borosilicate glass capillaries (GC150-10; Clark Electrochemical Instruments) were pulled using a vertical puller. The pulled electrodes were then dried in an oven at 220°C overnight and silanized with tributylchlorosilane (catalog no. 90796; Fluka). After drying and cooling, electrodes were back filled with back-filling solutions (200 mM KCl for K^+, 500 mM NaCl for Na^+, and 500 mM $CaCl_2$ for Ca^{2+}). The tips of the respective electrodes were front filled with commercially available selectophore cocktails (catalog no. 60031 for K^+ and catalog no. 21048 for Ca^{2+}; both from Sigma-Aldrich). For Na^+ flux measurements, recently developed calixarene-based microelectrodes with superior Na^+ selectivity were used (Jayakannan et al., 2011). Electrodes were calibrated in sets of appropriate solutions (Shabala et al., 2006) and then used for measurements. Only electrodes with a slope above 50 mV per decade and correlation greater than 0.999 were used.

Ready-to-measure seedlings were taken from the growth containers, and their roots were immobilized in the measuring chamber and preconditioned in BSM for 30 min. The measuring chamber was mounted on a microscope stage, and electrode tips were positioned 40 μm from the root surface, with their tips aligned and separated by several micrometers, using a 3D micromanipulator. During the measurements, a computer-controlled stepper motor moved electrodes in a slow (5-s) square-wave cycle between the two positions, close to (40 μm) and away from (120 μm) the root surface. Steady-state ion fluxes were then recorded over a period of 5 min. Then, an appropriate treatment was administered and the kinetics of net ion fluxes were recorded for a further 60 min. Net ion fluxes were measured at two positions along the longitudinal root axes: at 2 mm (elongation zone; Fig. 1A) and at approximately 15 mm (mature zone) from the root tip.

Patch-Clamp Experiments

Epidermal root protoplasts were isolated by enzymatic digestion in enzyme solution containing 2% (w/v) cellulose (Yakult Honsha), 1.2% (w/v) cellulysin (Biosciences), 0.1% (w/v) pectolyase, 0.1% (w/v) bovine serum albumin, 10 mM KCl, 10 mM $CaCl_2$, and 2 mM $MgCl_2$, pH 5.7, adjusted with 2 mM MES, with osmolality set hypertonic (780 mosmol; set with sorbitol) with respect to the cell sap. After a 30-min incubation of root segments either from the mature or distal elongation zone at 30°C on a 90-rpm rotary shaker, the preparation was rinsed with the same solution without enzymes and placed in a measuring chamber filled with a hypotonic (380 mosmol) solution, containing 10 mM KCl, 2 mM $CaCl_2$, and 1 mM $MgCl_2$, pH 5.7. After removing the root debris, released protoplasts were washed by a solution applied for patch-clamp assays (see below), and those attached for the bottom were used for further experiments. Protoplasts with a whole-cell capacitance of 5 to 10 pF (of epidermal origin; for justification, see Chen et al., 2007) were used in the experiments. Measurements were made by means of an Axopatch 200A patch-clamp amplifier (Axon Instruments). The patch-pipette were pulled in several steps on a Flaming-Brown P-97 micropipette puller (Sutter Instruments) and fire polished on an L/M CPZ-101 microforge (List-Medical), yielding final resistance in standard bath/pipette solutions of 5 to 8 MΩ. Protoplasts were patch clamped within 15 min after their release, and a new batch of protoplasts was used in each experiment. Once stable and low-leak ($R_{leak} > 5$ GΩ) whole-cell recording was established for approximately 15 min, a copper/ascorbate mixture (0.3/1 mM) was added directly to the bath to generate $OH^{\bullet}$. The pipette solution contained (in mM) 100 KOH-HEPES (pH 7.4), 3 $MgCl_2$, 0.8 $CaCl_2$, and 2 K_2EGTA; bath solution contained (in mM) 5 KCl, 2 $CaCl_2$, 0.5 $MgCl_2$, and 2 MES-KOH (pH 6), or the same plus 80 mM NaCl (at the end of treatment). All patch solutions were adjusted to 500 to 560 mosmol by variable additions of sorbitol.

Membrane Potential Measurements

A conventional microelectrode (GC 150F-10; Harvard Apparatus) with a tip diameter of approximately 0.5 μm was filled with 0.5 M KCl and connected to a microelectrode ion flux estimation electrometer via a silver/silver chloride half-cell. The mounted electrode was then impaled into the external cortex cells in either apical or mature root zones. Resting membrane potential measurements were recorded for 1 min before administering the treatment, and the resulting change in transient membrane potential was monitored continuously for up to 30 min. At least six individual plants were measured for each zone/treatment.

Intracellular Na^+ Distribution

Cytosolic and vacuolar Na^+ content in barley roots was quantified using the green fluorescent Na^+ dye CoroNa Green acetoxymethyl ester (Molecular Probes) essentially as described by Wu et al. (2015). In brief, the CoroNa Green indicator stock was added to 5 mL of measuring buffer (10 mM KCl and 5 mM Ca^{2+}-MES, pH 6.1) and diluted to a final concentration of 15 mM. Appropriate root segments were cut from the apical and mature root zones and incubated for 2 h in the dark in a solution containing 20 μM CoroNa Green. After incubation, the samples were rinsed in a buffered MES solution and examined using confocal microscopy. Confocal imaging was performed using an upright SP5 laser scanning confocal microscope (Leica Microsystems) equipped with a 40× oil-immersion objective. The excitation wavelength was set at 488 nm, and the emission was detected at 510 to 520 nm. Six to eight roots from individual plants were used, and a minimum of two images were taken for each root zone. On average, readings from between 70 and 300 cells were averaged and reported for each zone (Fig. 2). For analysis, several lines were drawn across the so-called region of interest in an appropriate root zone. Continuous fluorescence intensity distribution profiles (quantified in arbitrary units by LAS software) were then obtained and plotted in an Excel file. The mean fluorescence intensity values for cytosolic and vacuolar compartments were then calculated for each cell by attributing signal profiles to root morphology (visualized by light microscopy images). Special attention was paid to the fact that apical root cells may contain multiple vacuoles. The data were then averaged for all cells measured for the same treatment. The background signal was measured from the empty region and then subtracted from the readings to obtain corrected fluorescence values.

PM Isolation and H^+ Transport Activity

Seven-day-old barley seedlings were treated with either salt (NaCl; 100 mM) or water (control) for 24 h. Root apical and mature segments were cut. PMs were purified by two-phase partitioning as described in our previous publication (Pottosin et al., 2014). Proton pumping was measured by the quenching of ACMA (Lund and Fuglsang, 2012). PMs containing the H^+-ATPase were incubated with ATP (3 mM), and proton pumping was activated by the addition of magnesium in roots treated with 100 mM NaCl for 24 h compared with control roots. A total of 10 μg of PM protein was used for each analysis. The initial decrease in fluorescence after the addition of Mg^{2+} was a direct effect of the amount of protons transported into the vesicles by the H^+-ATPase.

ROS Detection

Apical (10 mm) and mature root sections were washed in 10 mM Tris-HCl buffer and incubated for 30 min at 37°C with 25 μM 2′,7′-dichlorofluorescein diacetate (Sigma-Aldrich) assayed as described by Rodrigo-Moreno et al. (2013). ROS levels (in arbitrary units) were measured with the software Image-Pro Plus 6.0 (Media Cybernetics).

Metabolite Extraction, Derivatization, and GC-MS Analysis

Five-millimeter-long root segments were isolated from apical and mature zones, and approximately 20 mg of each tissue (exact fresh weight recorded) was transferred into prechilled cryomill tubes (2 mL; 1.4-mm CK14 Ceramic Bead Kit; Sapphire Bioscience) and rapidly frozen in liquid nitrogen. A total of 100 μL of 100% methanol was added to the root tissue, containing 5 μL of internal standard solution (1 mg mL^{-1} [$^{13}C_6$]sorbitol and L-[$^{13}C_5$,^{15}N]Val). The tissue in the solution was homogenized using an automatic mill (Precellys 24) running at 6,400 rpm for 30 s followed by incubation at 70°C for 15 min. A further 100 μL of water was added to root extracts. After centrifugation at 13,000 rpm, an aliquot of 60 μL of the extract was taken and dried in vacuo for subsequent derivatization with *N*-methyl-*N*-(*tert*-butyldimethylsilyl)trifluoroacetamide + 1% *tert*-butyldimethylchlorosilane. An second aliquot of 70 μL of the extracts was taken and dried in vacuo for subsequent derivatization with *N*,*O*-bis(trimethylsilyl)trifluoroacetamide with 1% trimethylchlorosilane (Sigma-Aldrich). The dried extracts were

redissolved and derivatized prior to injection using a Gerstel 2.5.2 autosampler for 120 min at 37°C (10 μL of 30 mg mL^{-1} methoxyamine hydrochloride in pyridine) followed by treatment with 20 μL of trimethylchlorosilane or *tert*-butyldimethylchlorosilane and 2 μL of a retention time standard mixture (0.029% [v/v] *n*-dodecane, *n*-pentadecane, *n*-nonadecane, *n*-docosane, *n*-octacosane, *n*-dotriacontane, and *n*-hexatriacontane dissolved in pyridine; all Sigma-Aldrich) for another 30 min at 37°C. GC-MS data acquisition and data analysis were carried out exactly as described earlier (Hill et al., 2013).

Supplemental Data

The following supplemental materials are available.

Supplemental Figure S1. A multicompartment chamber allowing imposition to a specific root zone.

Supplemental Figure S2. Pharmacological evidence for NSCC channels mediating NaCl-induced K^+ efflux in the root apex.

ACKNOWLEDGMENT

We thank Anette Lund for technical help.

Received September 7, 2016; accepted October 14, 2016; published October 21, 2016.

LITERATURE CITED

Adem GD, Roy SJ, Zhou M, Bowman JP, Shabala S (2014) Evaluating contribution of ionic, osmotic and oxidative stress components towards salinity tolerance in barley. BMC Plant Biol **14:** 113

Anschütz U, Becker D, Shabala S (2014) Going beyond nutrition: regulation of potassium homoeostasis as a common denominator of plant adaptive responses to environment. J Plant Physiol **171:** 670–687

Bose J, Rodrigo-Moreno A, Lai D, Xie Y, Shen W, Shabala S (2015) Rapid regulation of the plasma membrane H^+-ATPase activity is essential to salinity tolerance in two halophyte species, Atriplex lentiformis and Chenopodium quinoa. Ann Bot (Lond) **115:** 481–494

Chen Z, Newman I, Zhou M, Mendham N, Zhang G, Shabala S (2005) Screening plants for salt tolerance by measuring K^+ flux: a case study for barley. Plant Cell Environ **28:** 1230–1246

Chen Z, Pottosin II, Cuin TA, Fuglsang AT, Tester M, Jha D, Zepeda-Jazo I, Zhou M, Palmgren MG, Newman IA, et al (2007) Root plasma membrane transporters controlling K^+/Na^+ homeostasis in salt-stressed barley. Plant Physiol **145:** 1714–1725

Cuin TA, Shabala S (2007) Compatible solutes reduce ROS-induced potassium efflux in Arabidopsis roots. Plant Cell Environ **30:** 875–885

Demidchik V (2015) Mechanisms of oxidative stress in plants: from classical chemistry to cell biology. Environ Exp Bot **109:** 212–228

Demidchik V, Cuin TA, Svistunenko D, Smith SJ, Miller AJ, Shabala S, Sokolik A, Yurin V (2010) Arabidopsis root K^+-efflux conductance activated by hydroxyl radicals: single-channel properties, genetic basis and involvement in stress-induced cell death. J Cell Sci **123:** 1468–1479

Demidchik V, Maathuis FJM (2007) Physiological roles of nonselective cation channels in plants: from salt stress to signalling and development. New Phytol **175:** 387–404

Demidchik V, Shabala SN, Davies JM (2007) Spatial variation in H_2O_2 response of Arabidopsis thaliana root epidermal Ca^{2+} flux and plasma membrane Ca^{2+} channels. Plant J **49:** 377–386

Demidchik V, Straltsova D, Medvedev SS, Pozhvanov GA, Sokolik A, Yurin V (2014) Stress-induced electrolyte leakage: the role of K^+-permeable channels and involvement in programmed cell death and metabolic adjustment. J Exp Bot **65:** 1259–1270

Dinneny JR (2010) Analysis of the salt-stress response at cell-type resolution. Plant Cell Environ **33:** 543–551

Dinneny JR, Long TA, Wang JY, Jung JW, Mace D, Pointer S, Barron C, Brady SM, Schiefelbein J, Benfey PN (2008) Cell identity mediates the response of Arabidopsis roots to abiotic stress. Science **320:** 942–945

Dubey RS, Rani M (1990) Influence of NaCl salinity on the behavior of protease, aminopeptidase and carboxypeptidase in rice seedlings in relation to salt tolerance. Aust J Plant Physiol **17:** 215–221

Flowers TJ (2004) Improving crop salt tolerance. J Exp Bot **55:** 307–319

Flowers TJ, Munns R, Colmer TD (2015) Sodium chloride toxicity and the cellular basis of salt tolerance in halophytes. Ann Bot (Lond) **115:** 419–431

Forde BG (2014) Glutamate signalling in roots. J Exp Bot **65:** 779–787

Hill CB, Jha D, Bacic A, Tester M, Roessner U (2013) Characterization of ion contents and metabolic responses to salt stress of different Arabidopsis AtHKT1;1 genotypes and their parental strains. Mol Plant **6:** 350–368

Hirsch RE, Lewis BD, Spalding EP, Sussman MR (1998) A role for the AKT1 potassium channel in plant nutrition. Science **280:** 918–921

Jayakannan M, Babourina O, Rengel Z (2011) Improved measurements of Na^+ fluxes in plants using calixarene-based microelectrodes. J Plant Physiol **168:** 1045–1051

Ji H, Pardo JM, Batelli G, Van Oosten MJ, Bressan RA, Li X (2013) The Salt Overly Sensitive (SOS) pathway: established and emerging roles. Mol Plant **6:** 275–286

Julkowska MM, Testerink C (2015) Tuning plant signaling and growth to survive salt. Trends Plant Sci **20:** 586–594

Keunen E, Peshev D, Vangronsveld J, Van Den Ende W, Cuypers A (2013) Plant sugars are crucial players in the oxidative challenge during abiotic stress: extending the traditional concept. Plant Cell Environ **36:** 1242–1255

Kurusu T, Kuchitsu K, Tada Y (2015) Plant signaling networks involving Ca^{2+} and Rboh/Nox-mediated ROS production under salinity stress. Front Plant Sci **6:** 427

Lecourieux D, Mazars C, Pauly N, Ranjeva R, Pugin A (2002) Analysis and effects of cytosolic free calcium increases in response to elicitors in *Nicotiana plumbaginifolia* cells. Plant Cell **14:** 2627–2641

Liszkay A, van der Zalm E, Schopfer P (2004) Production of reactive oxygen intermediates ($O_2^{\cdot-}$, H_2O_2, and $^{\cdot}OH$) by maize roots and their role in wall loosening and elongation growth. Plant Physiol **136:** 3114–3123, discussion 3001

Lund A, Fuglsang AT (2012) Purification of plant plasma membranes by two-phase partitioning and measurement of H^+ pumping. Methods Mol Biol **913:** 217–223

Ma S, Bohnert HJ (2007) Integration of *Arabidopsis thaliana* stress-related transcript profiles, promoter structures, and cell-specific expression. Genome Biol **8:** R49

Ma S, Gong Q, Bohnert HJ (2006) Dissecting salt stress pathways. J Exp Bot **57:** 1097–1107

Mittler R (2002) Oxidative stress, antioxidants and stress tolerance. Trends Plant Sci **7:** 405–410

Palmgren MG, Nissen P (2011) P-type ATPases. Annu Rev Biophys **40:** 243–266

Pottosin I, Velarde-Buendía AM, Bose J, Fuglsang AT, Shabala S (2014) Polyamines cause plasma membrane depolarization, activate Ca^{2+}-, and modulate H^+-ATPase pump activity in pea roots. J Exp Bot **65:** 2463–2472

Price MB, Jelesko J, Okumoto S (2012) Glutamate receptor homologs in plants: functions and evolutionary origins. Front Plant Sci **3:** 235

Qadir M, Quillérou E, Nangia V, Murtaza G, Singh M, Thomas RJ, Drechsel P, Noble AD (2014) Economics of salt-induced land degradation and restoration. Nat Resour Forum **38:** 282–295

Rodrigo-Moreno A, Andrés-Colás N, Poschenrieder C, Gunsé B, Peñarrubia L, Shabala S (2013) Calcium- and potassium-permeable plasma membrane transporters are activated by copper in Arabidopsis root tips: linking copper transport with cytosolic hydroxyl radical production. Plant Cell Environ **36:** 844–855

Rodríguez AA, Maiale SJ, Menédez AB, Ruiz OA (2009) Polyamine oxidase activity contributes to sustain maize leaf elongation under saline stress. J Exp Bot **60:** 4249–4262

Roy SJ, Negrão S, Tester M (2014) Salt resistant crop plants. Curr Opin Biotechnol **26:** 115–124

Sagi M, Omarov RT, Lips SH (1998) The Mo-hydroxylases xanthine dehydrogenase and aldehyde oxidase in ryegrass as affected by nitrogen and salinity. Plant Sci **135:** 125–135

Shabala L, Cuin TA, Newman IA, Shabala S (2005) Salinity-induced ion flux patterns from the excised roots of Arabidopsis sos mutants. Planta **222:** 1041–1050

Shabala L, Ross T, McMeekin T, Shabala S (2006a) Non-invasive microelectrode ion flux measurements to study adaptive responses of microorganisms to the environment. FEMS Microbiol Rev **30:** 472–486

Shabala S (2009) Salinity and programmed cell death: unravelling mechanisms for ion specific signalling. J Exp Bot **60:** 709–712

Shabala S (2013) Learning from halophytes: physiological basis and strategies to improve abiotic stress tolerance in crops. Ann Bot (Lond) **112:** 1209–1221

Shabala S, Demidchik V, Shabala L, Cuin TA, Smith SJ, Miller AJ, Davies JM, Newman IA (2006b) Extracellular Ca^{2+} ameliorates NaCl-induced K^+ loss from Arabidopsis root and leaf cells by controlling plasma membrane K^+-permeable channels. Plant Physiol **141:** 1653–1665

Shabala S, Pottosin I (2014) Regulation of potassium transport in plants under hostile conditions: implications for abiotic and biotic stress tolerance. Physiol Plant **151:** 257–279

Shabala SN, Lew RR (2002) Turgor regulation in osmotically stressed Arabidopsis epidermal root cells: direct support for the role of inorganic ion uptake as revealed by concurrent flux and cell turgor measurements. Plant Physiol **129:** 290–299

Shelden MC, Dias DA, Jayasinghe NS, Bacic A, Roessner U (2016) Root spatial metabolite profiling of two genotypes of barley (*Hordeum vulgare* L.) reveals differences in response to short-term salt stress. J Exp Bot **67:** 3731–3745

Shi H, Ishitani M, Kim C, Zhu JK (2000) The *Arabidopsis thaliana* salt tolerance gene SOS1 encodes a putative Na^+/H^+ antiporter. Proc Natl Acad Sci USA **97:** 6896–6901

Shi H, Quintero FJ, Pardo JM, Zhu JK (2002) The putative plasma membrane Na^+/H^+ antiporter SOS1 controls long-distance Na^+ transport in plants. Plant Cell **14:** 465–477

Sohn JW (2013) Ion channels in the central regulation of energy and glucose homeostasis. Front Neurosci **7:** 85

Stephens NR, Qi Z, Spalding EP (2008) Glutamate receptor subtypes evidenced by differences in desensitization and dependence on the GLR3.3 and GLR3.4 genes. Plant Physiol **146:** 529–538

Sun Y, Kong X, Li C, Liu Y, Ding Z (2015) Potassium retention under salt stress is associated with natural variation in salinity tolerance among Arabidopsis accessions. PLoS ONE **10:** e0124032

Tester M, Davenport R (2003) Na^+ tolerance and Na^+ transport in higher plants. Ann Bot (Lond) **91:** 503–527

Velarde-Buendía AM, Shabala S, Cvikrova M, Dobrovinskaya O, Pottosin I (2012) Salt-sensitive and salt-tolerant barley varieties differ in the extent of potentiation of the ROS-induced K^+ efflux by polyamines. Plant Physiol Biochem **61:** 18–23

Verdoucq L, Rodrigues O, Martinière A, Luu DT, Maurel C (2014) Plant aquaporins on the move: reversible phosphorylation, lateral motion and cycling. Curr Opin Plant Biol **22:** 101–107

Véry AA, Nieves-Cordones M, Daly M, Khan I, Fizames C, Sentenac H (2014) Molecular biology of K^+ transport across the plant cell membrane: what do we learn from comparison between plant species? J Plant Physiol **171:** 748–769

Wang P, Kong CH, Sun B, Xu XH (2012) Distribution and function of allantoin (5-ureidohydantoin) in rice grains. J Agric Food Chem **60:** 2793–2798

Watanabe S, Matsumoto M, Hakomori Y, Takagi H, Shimada H, Sakamoto A (2014) The purine metabolite allantoin enhances abiotic stress tolerance through synergistic activation of abscisic acid metabolism. Plant Cell Environ **37:** 1022–1036

Widodo, Patterson JH, Newbigin E, Tester M, Bacic A, Roessner U (2009) Metabolic responses to salt stress of barley (Hordeum vulgare L.) cultivars, Sahara and Clipper, which differ in salinity tolerance. J Exp Bot **60:** 4089–4103

Wu H, Shabala L, Liu X, Azzarello E, Zhou M, Pandolfi C, Chen ZH, Bose J, Mancuso S, Shabala S (2015) Linking salinity stress tolerance with tissue-specific Na+ sequestration in wheat roots. Front Plant Sci **6:** 71